Precambrian Research 280 (2016) 31–45

Contents lists available at ScienceDirect

Precambrian Research

journal homepage: www.elsevier.com/locate/precamres

Neoproterozoic sedimentary basin evolution in southwestern Tarim, NW China: New evidence from field observations, detrital zircon U–Pb ages and Hf isotope compositions

Chuan-Lin Zhang [a,*], Xian-Tao Ye [b], Hai-Bo Zou [c], Xiang-Yan Chen [b]

[a] College of Oceanography, Hohai University, Nanjing 210098, PR China
[b] Nanjing Institute of Geology and Mineral Resources, Nanjing 210016, PR China
[c] Department of Geosciences, Auburn University, Auburn, AL 36849-5305, USA

ARTICLE INFO

Article history:
Received 15 March 2016
Revised 24 April 2016
Accepted 27 April 2016
Available online 4 May 2016

Keywords:
Southwestern Tarim
Neoproterozoic sedimentary basins
Detrital zircon U–Pb ages
Zircon Hf isotope compositions
Tectonic evolution

ABSTRACT

Sedimentary basin evolution is intimately related to tectonic background and thus can serve as one of the most important indicators in deciphering the regional tectonic evolution process. Neoproterozoic volcanic-sedimentary sequences are well preserved along the southwestern margin of the Tarim Block in NW China and provide new insights into the Neoproterozoic tectonic evolution of the Tarim. In this contribution, we report the metamorphic deformation features and systematic detrital zircon U–Pb ages and Hf isotope compositions of the Neoproterozoic strata in SW Tarim. Geochronological data reveal that the greenschist-facies metamorphic and tightly folded Sailajiazitage Group (SG) volcanic-sedimentary sequence deposited during 860–830 Ma, the Ailiankate Group (AG) clastic rocks of low greenschist – facies metamorphism and intensive deformation deposited during 820–800 Ma, and the unmetamorphosed and undeformed late Neoproterozoic carbonate–clastic–tillite sequences, including the Silu Group (SLG) and the Qiakemakelieke Group (QG), deposited after 760 Ma. Two phases of glaciations from the QG in SW Tarim could be equivalent to the Beiyixi glaciation and the Altungol–Tereeken glaciation in north Tarim, respectively. Rock assemblages coupled with geochemistry of the SG bimodal volcanic rocks indicate its deposition in a back-arc basin. Rock assemblages, detrital zircon age spectra and its metamorphism and deformation features suggest that the AG clastic sequence most likely deposited at a foreland basin on the back-arc basin sedimentary package while the middle to late Neoproterozoic SLG and QG carbonate–clastic–tillite sequences deposited at a passive marginal and/or rift basins. The Neoproterozoic evolution process of the southwestern Tarim demonstrates that (1) the Neoproterozoic assemblage of the Tarim basement could have lasted till 760 Ma as evidenced by the Aksu blueschist-facies metamorphism and (2) its Pre-Nanhuaian basement could be composed of independent continental terranes. Furthermore, positive $\varepsilon Hf(t)$ deviations in these detrital zircons suggest that the Rodinia plume could have effects on the Neoproterozoic igneous activities.

1. Introduction

Detrital zircon geochronology and geochemistry is becoming a powerful method in deciphering sedimentary provenance and in crustal evolution (e.g., Kemp et al. (2006), Cawood et al. (2007a, b), Grove et al. (2008a,b), Hawkesworth et al. (2010), Li et al. (2014), Gehrels (2014), Spencer et al. (2015)), owing to zircon's refractory characteristics during metamorphic and weathering processes (Zheng et al., 2007), and the availability of large numbers of in situ, high precision analyses of their ages, trace elements, oxygen and Lu–Hf isotope compositions using modern microbeam techniques (ion probe and LA-MC/Q-ICPMS, e.g., Liu et al. (2008), Li et al. (2014)). Detrital zircon spectra have distinctive age distribution patterns that reflect the tectonic setting of the basin in which they are deposited, and could provide a framework that can be used to constrain the tectonic setting of sedimentary packages (Cawood et al., 2012). In addition, systematic in situ zircon Lu–Hf isotope compositions, coupled with in situ U–Pb ages, have been widely used to discuss regional tectonic evolution and the continental growth process (e.g., Kemp et al. (2006), Condie et al. (2009a,b); Sun et al., 2009; Li et al., 2014).

The Tarim Craton in the Xinjiang Uygur Autonomous Region of northwestern China, covering an area of more than 600,000 km^2, is

* Corresponding author. Tel.: +86 25 84897863; fax: +86 25 84600446.
E-mail address: zchuanlin1968@gmail.com (C.-L. Zhang).

http://dx.doi.org/10.1016/j.precamres.2016.04.011
0301-9268/

one of the main three Precambrian nuclei in China (i.e., Tarim, North China and South China) (Zhao and Cawood, 2012; Zheng et al., 2013; Zhang et al., 2013). The craton is surrounded by the Phanerozoic orogenic belts of Tienshan Mountains to the north, the western Kunlun Mountains to the south, and the Central-Southern Altyn Tagh Mountains to the southeast (Fig. 1a). In recent years, many studies focusing on the Neoproterozoic geology of Tarim illustrated that the craton was assembled within the Rodinia supercontinent during late Mesoproterozoic to early-middle Neoproterozoic (Zhang et al., 2003a, 2012a; Zhan et al., 2007; Lu et al., 2008; Shu et al., 2011; He et al., 2012). The two main pulses of Neoproterozoic magmatism at 820–800 Ma and 780–760 Ma were considered to be related to the Rodinian plume (Zhang et al., 2007a,b, 2009, 2011, 2012b; Xu et al., 2005, 2009, 2013; Zhu et al., 2008). Several studies on the early Precambrian history of this craton show 2.0–1.8 Ga metamorphism overprinted on the Archean and Paleoproterozoic outcropping along the northern margin (the Quruqtagh terrane), the southwestern Tarim terrane and the Altyn terrane in the east, which was considered to be correlated to the assembly of the Columbia supercontinent (Lu et al., 2008; Shu et al., 2011; Long et al., 2010, 2011; Zhang et al., 2011; Ge et al., 2013a, 2013b). Recently, Zhang et al. (2014a) and Ye et al. (2016) suggested that the Precambrian basement of the Tarim possibly composed of discrete terranes drifted from different Precambrian nuclei and these terranes did not assemble until the early to middle Neoproterozoic during the assemblage of the Rodinia supercontinent.

Although many studies have been carried on the Neoproterozoic igneous activities in Tarim, little attention has been paid to the tectonic settings of the Neoproterozoic sedimentary basins (Turner, 2010). In order to evaluate the coupling between Neoproterozoic tectonic evolution process and the development of sedimentary basins along the southwestern margin of the Tarim, in this contribution, we analyzed U–Pb ages and Hf isotope compositions of the detrital zircons from different Neoproterozoic members outcropping in southwestern Tarim. Using these data, in combination with metamorphic and deformation features of these members observed in the field, we aim to: (1) decipher the tectonic settings of the Neoproterozoic basin and the possible tectonic system transformation from early to late Neoproterozoic in southwestern Tarim; (2) describe a more detailed late Mesoproterozoic to Neoproterozoic tectonic evolution process of the southwestern Tarim terrane; and (3) constrain the Neoproterozoic glaciation age for a better correlation of the glaciation at the different terranes of the Tarim.

2. Regional geology

The Tarim Craton is bound by the Tianshan, western Kunlun and Central-Southern Altyn-Tagh Mountain belts to the north, south and southeast, respectively (Fig. 1a) (Lu et al., 2008; Zhang et al., 2013). The craton shows typical double-layered structure sequence consisting of a Precambrian basement (pre-Neoproterozoic or Pre-Nanhuaian) and a late Neoproterozoic to Cambrian cover (Lu, 1992; Xinjiang, 1993; Feng et al., 1995; Gao and Chen, 2003). The Precambrian rocks in the Tarim Craton are mostly exposed along the northern, eastern and southwestern margins. In central Tarim, Precambrian igneous and metamorphic rocks were obtained in the drilling holes (Li et al., 2005; Guo et al., 2005; Xu et al., 2013a,b).

The major Precambrian rock series of the southwestern Tarim terrane (STT) are mainly composed of the Paleoproterozoic Heluositan complex and the 2.41 Ga Akazi pluton (Zhang et al., 2007c; Wang et al., 2014; Ye et al., 2016) (Fig. 2), the Mesoproterozoic greenschist- to amphibolite- facies metamorphosed and intensively folded sedimentary sequences, and the Neoproterozoic volcanic-sedimentary sequences and carbonate–clastic–tillite

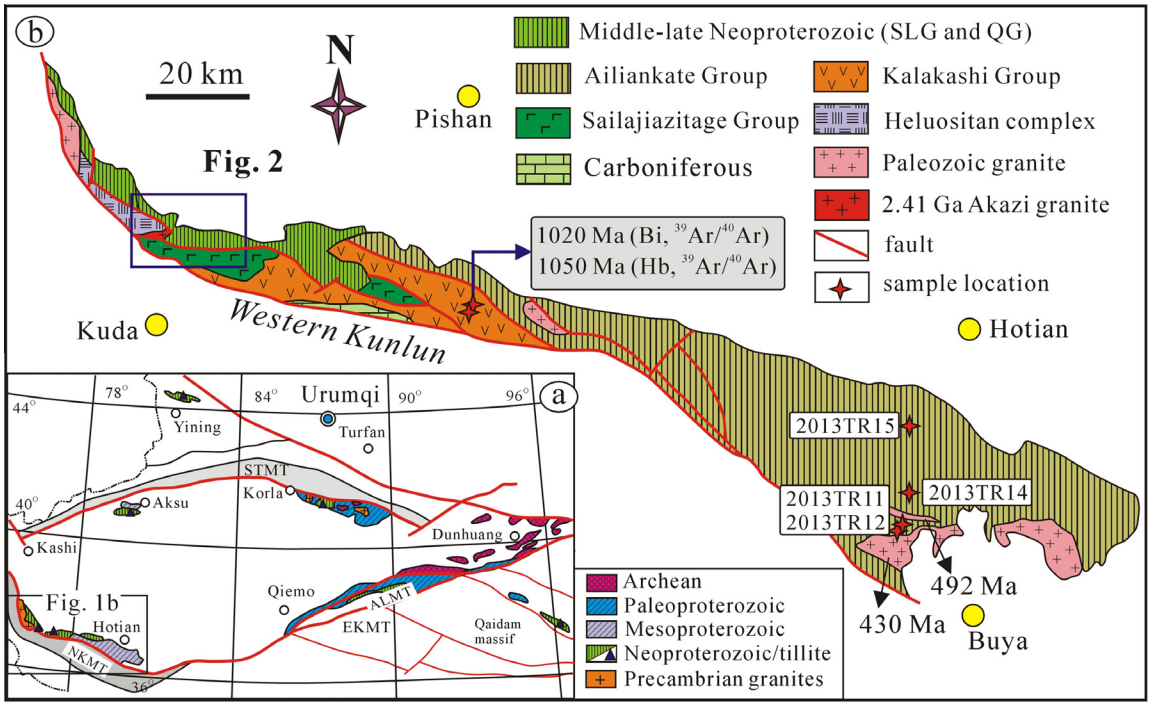

Fig. 1. (a) Tectonic framework of the Tarim Craton and its adjacent areas showing the Precambrian terranes along its margin. (b) Main Precambrian unites in the southwestern section of the Tarim Craton. Hornblende and biotite $^{39}Ar/^{40}Ar$ plateau ages are marked for the high greenschist to amphibolite facies metamorphic Mesoproterozoic Kalakashi Group (modified after Xinjiang (1993)). The Neoproterozoic sequences could be divided into main three members, i.e., member 1, the Sailajiazitage group; member 2, the Ailiankate Group and member 3, the Silu Group (SLG) and Qiakemakelieke Group (QG). Both member 1 and member 2 underwent low greenschist-facies metamorphism and intensive deformation while member 3, of no deformation and metamorphism.

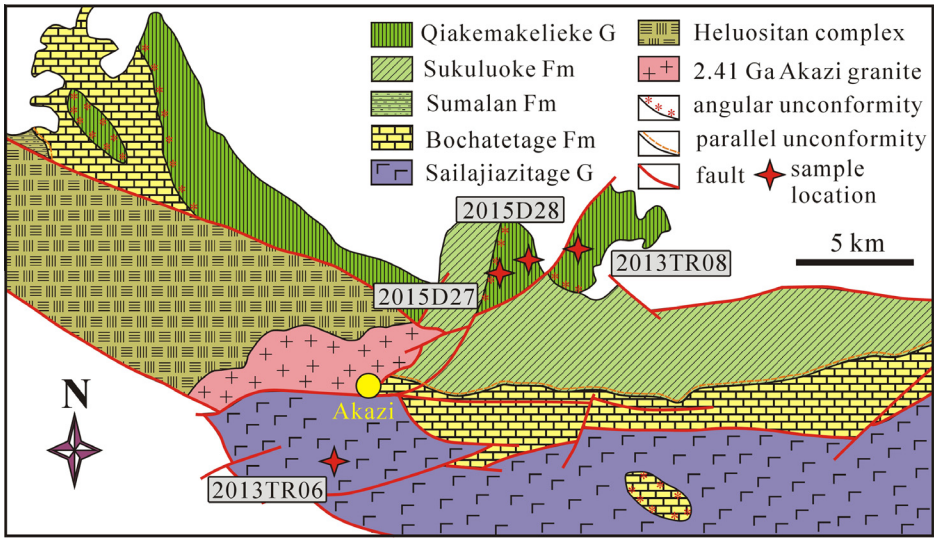

Fig. 2. Geological map of the Neoproterozoic sequences along the Xinjiang–Tibet road (see details in the text).

Fig. 3. Representative field photographs of the studied Neoproterozoic sequences. (a, b) The Ailiankate Group, showing the felsic (minor carbonate) dykes paralleling with the schistosity, indicating these dykes were formed during metamorphic differentiation; (c) a fine-grained granite sheet intrude the clastic rocks, zircon U–Pb age of the granite is marked; (d) the parallel cleavage in the gravel from the BF tillite; (e) the BF tillite; (f) a sandstone layer in the BF tillite (sample 2015D28 was collected from this layer).

sequences without significant metamorphism and deformation (Zhang et al., 2010) (Fig. 1b). The Heluositan complex mainly consists of gneissic granites, orthogneisses and migmatites which underwent ca.1.9 Ga amphibolite to granulite facies metamorphism (Zhang et al., 2007c; Guo et al., 2013; Wang et al., 2014). The Kalakashi Group (KG) and the Ailiankate Group (AG) were considered as Paleoproterozoic by local geologists (Xinjiang BGMR; Wang, 2000), but recent studies revealed that they are late Mesoproterozoic (KG) and Neoproterozoic (AG), respectively (Zhang et al., 2003a; Wang et al., 2015, see following discussions). The KG, which underwent high greenschist–amphibolite facies metamorphism and strong deformation, is the most reliable late Mesoproterozoic sequence composed by approximately equal volumes of volcanic rocks and clastic rocks, possibly deposited during 1.2–1.0 Ga according to Sm–Nd isochron and hornblende and biotite $^{39}Ar/^{40}Ar$ plateau ages (Fig. 1b) (Zhang et al., 2003b). The metamorphic ages of the KG were suggested to be related the assemblage of the southern Tarim terrane to the Rodinia supercontinent (Zhang et al., 2003b).

3. Field observations and sample collections

The Sailajiazitage Group (SG), mainly outcropping along the Xinjiang–Tibet road, was considered as Mesoproterozoic by local geologists (Xinjiang, 1993). It contacts with the 2.34 Ga Heluositan complex with fault and is unconformably covered by the Neoproterozoic Bochatetage Formation (BCF) (Fig. 2) (Zhang et al., 2007c; Ye et al., 2016). The SG mainly composes of volcanic-sedimentary sequences including basalts, rhyolite, tuff-bearing clastic rocks, siltstone and immature sandstone (Guo et al., 2004; Wang et al., 2015). The bimodal volcanic rocks account for about half of the total thickness of the SG in line with the geological profile along the Xinjiang–Tibet road (Guo et al., 2004).

The widely distributed AG at the eastern section of the STT mainly composes of clastic rocks and underwent low greenschist facies metamorphism and tightly folded deformation. At its southern margin it contacts with the early Paleozoic Northern Kunlun orogen by the Tiekelike Fault and intruded by the ca.430 Ma Buya granites (Fig. 1b) (Ye et al., 2008). The AG sedimentary sequence is excellently exposed along the more than 100 km Hotian-Buya road. In line with field observations, the main rocks include sericite–chlorite (quartz) schist, siltstone, fine-grained sandstone and plagioclase–quartz greywacke. Low greenschist facies metamorphic minerals such as biotite, sericite and chlorite are commonly seen in most rock types. At the southern part of this sedimentary sequence, felsic dykes of 20–50 cm long and 2–10 cm wide, almost paralleling with the foliations, were observed (Fig. 3a, and b). A fine-grained granite sheet (zircons yield concordant U–Pb age of 492 ± 3 Ma, our unpublished data) intrudes the AG (Fig. 3c). Due to its tight folding, the precise thickness of the AG sedimentary sequence is unknown. Nevertheless, recent regional mapping revealed that its thickness is at least up to 3000 m (Xinjiang, 1993; Zhang et al., 2007b)

The unmetamorphosed and undeformed carbonate–clastic–tillite Neoproterozoic sequence in southwestern Tarim, was divided into two groups, i.e., the Silu Group (SLG) and the Qiakemakelieke Group (QG). The SLG include Bochatetage Formation (BCF), Sumalan Formation (SMF) and Sukuluoke Formation (SKF) in an ascending order, and mainly compose of diverse type of clastic rocks and carbonate (Ma et al., 1989, 1991; Wang et al., 2004) (Fig. 2). The QG, excellently outcrops nearby the Xinjiang–Tibet road, was divided into six formations as the Yalaguzi Formation (YLF), Bolong Formation (BF), Kexili Formation (KF), Yutang Formation (YTF), Kuerkake Formation (KKF) and Kezisuhumu Formation (KF), in an ascending order (Gao et al., 1985; Ma et al., 1991) (Fig. 4). The lowest YLF composes of conglomerate unconformably overlies on the

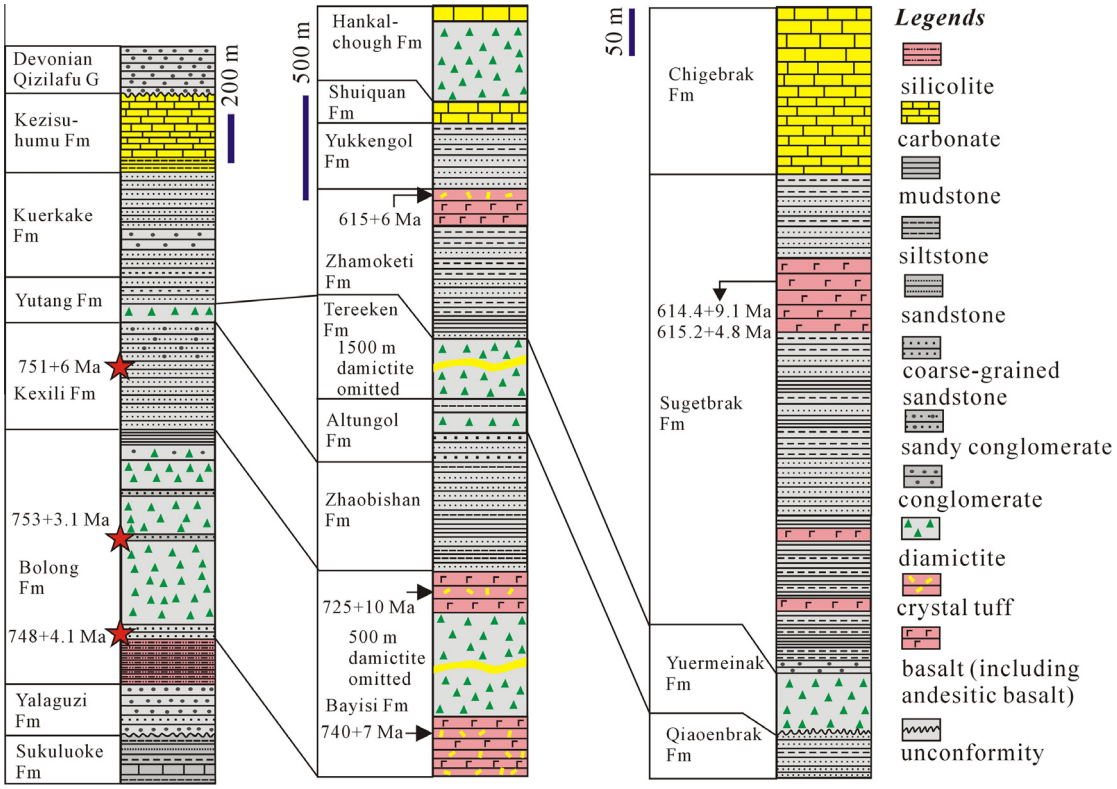

Fig. 4. Stratigraphic column of the tillite-bearing Qiakemakelieke Group in southwestern Tarim (modified after Ma et al. (1989, 1991) and the latest 1/50,000 mapping data) (the tillite-bearing Neoproterozoic sequences in Quruqtagh and in Aksu are also presented for comparison, after Xu et al. (2009, 2013a,b)).

SKF. Ca. 200 m silicolite occurs at the bottom of the BF, then 2 m of sandstone overlies on the silicolite. About 760 m tillite occurs in BF. The rock types of the glacial gravels include gneissic granite, massive granite, sandstone, silicolite, quartzite, schist, etc. The size of the gravels varies from 1 cm to 50 cm and mostly within 10–30 cm (Fig. 3d and e). Striae, saddle-shape gravels and cool shearing foliation of the gravels are commonly seen on outcrops (Fig. 3d and e). Two layers of sandstone (with minor siltstone) occur in the tillites (Fig. 3f). At the top of the BF is a 5 m siltstone layer. The lower part of the KF mainly composes of coarse-grained sandstone with minor thin-layered siltstone and the upper part is a sandy conglomerate sequence. The second phase of the tillite occurs at the lower part of the YTF, and shares most features of the tillite in the BF. The upper part of the YTF is ca.100 m sandstone. The KKF mainly composes of sandstone, siltstone with minor conglomerate. The KF mainly composes of carbonate (dolomite cap) with a 50 m siltstone interbedded with mudstone at its lower part. Devonian conglomerate unconformably overlies on the carbonate.

One sandy tuff sample was collected from the Sailajiazitage Group (2013TR06, 37°4′55″N, 76°55′5″E). In thin section, minor crystal fragments and detritus were observed (Fig. 5a). The matrix mainly composes of chlorite and sericite with some very fine felsic minerals (Fig. 5a). Four samples were collected from AG along the Hotian-Buya road. Sample 2013TR11 (36°29′18″N, 79°54′48″E) is a biotite plagioclase–quartz schist, composing 5% sericite, 25–30% biotite, 20–30% plagioclase and 40–50% quartz (Fig. 5b). Both sample 2013TR12 (36°29′29″N, 79°54′55″E) and 2013TR14 (36°32′13″N, 79°55′35″E) are feldspar–quartz sandstone (Fig. 5c and d), composing of minor sericite (generally less than 5%) and Ti–Fe oxide (~5%), 30–40% feldspar and 40–50% quartz (Fig. 5c and d). The quartz sandstone sample 2013TR15 (36°39′48″, 79°51′54″) was collected from the uppermost part of the AG, mainly composes of quartz (>80%) and minor feldspar and biotite (Fig. 5e). Three samples were collected from the QG, sample 2015D27 (37°7′54″N, 77°00′51″E) and sample 2015D28 (37°07′52″N, 77°00′53″E) were collected from the sandstone at lower part of the BF and the 40 cm thick sandstone layer occurring in the middle of the BF tillite, respectively. They share similar texture and mineral compositions (Fig. 5f–h). The detritus, variable in size, are of low psephicity and low degree of sorting. Some muddy sediments are seen in thin sections (Fig. 5g). Sample 2013TR08 (37°07′41″N, 77°01′37″E) was collected from the conglomerate-bearing sandstone of KXF. Main detritus include feldspar, quartz and some rock fragments (Fig. 5i).

4. Analytical methods

Zircon separation was carried out using conventional magnetic and density techniques to concentrate non-magnetic, heavy fractions. Zircon grains were then hand-picked under a binocular microscope. Zircon grains were mounted in epoxy mounts which

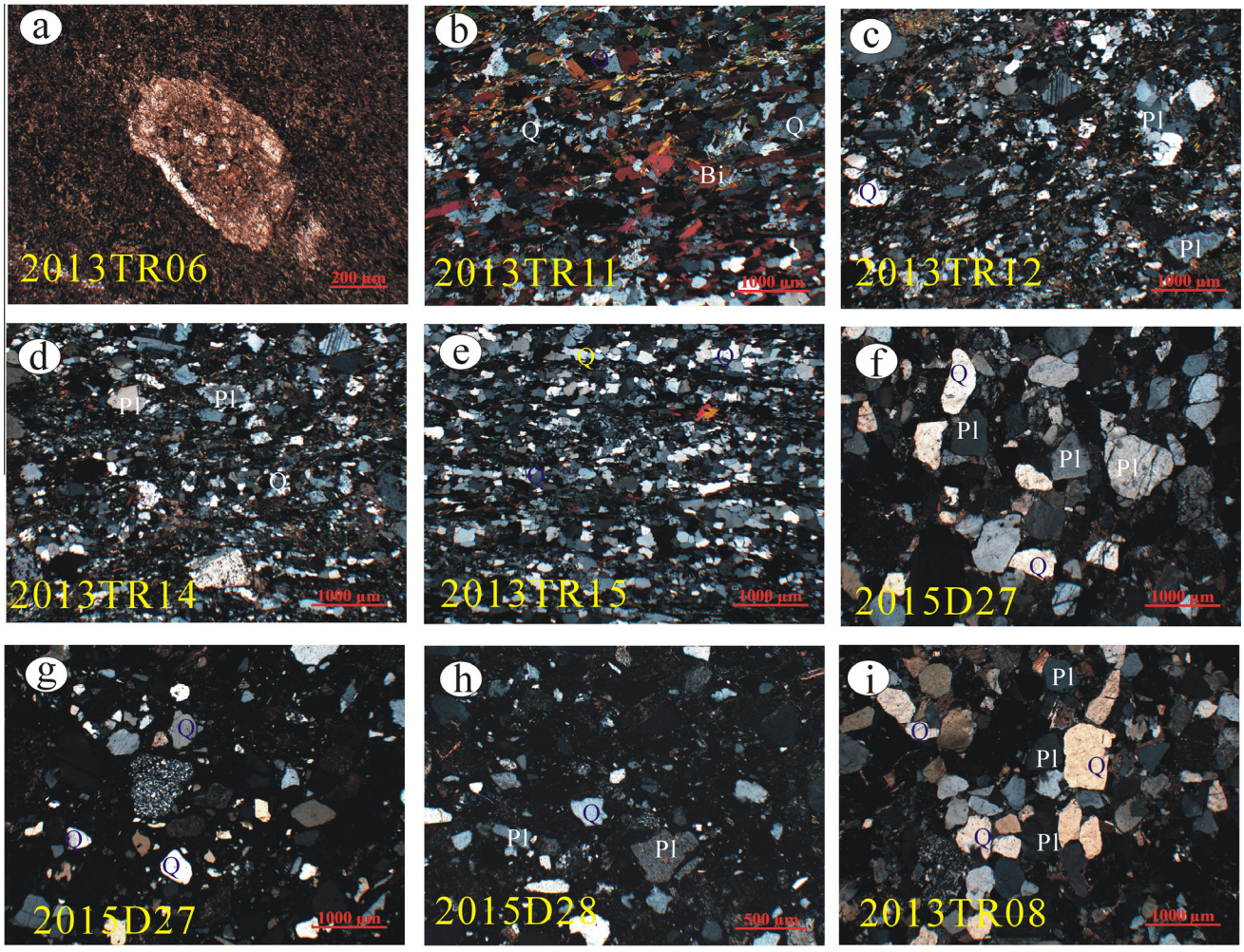

Fig. 5. Photomicrographs of the geochronological samples (see details in the text). Abbreviations: Bi-biotite, Q-quartz, Pl-plagioclase.

were then polished to section the crystals in half for analysis. All zircons were documented with transmitted and reflected light micrographs as well as cathodoluminescence (CL) images to reveal their internal structures. Zircon U–Pb ages and Hf isotope compositions were analyzed using the LA-ICP-MS method at the Tianjin Institute of Geology and Mineral Resources, Chinese Geological Survey. A Neptune MC-ICP-MS coupled with a 193 nm excimer laser ablation system were used to determine zircon U–Pb ages. The laser beam diameter was 35 μm and it was operated with a frequency of 10 Hz. Every set of five sample analyses was followed by analysis of the zircon standards 91,500 and eight sample analyses followed by the zircon standard GJ-1 (Jackson et al., 2004), and the glass standard NIST610 (see Hou et al., 2009). Each analysis consisted of ca.5 s of background data acquisition and 45 s of sample data acquisition. $^{207}Pb/^{206}Pb$, $^{206}Pb/^{238}U$, $^{207}Pb/^{235}U$, and $^{208}Pb/^{232}Th$ ratios were corrected for laser and instrumentally induced elemental and isotopic fractionation using zircon GJ-1 as an external standard. Common Pb was corrected using the method proposed by Andersen (2002). The U–Pb concordia plots were processed with ISOPLOT 3.0 and data are presented with 1σ errors and 95% confidence limits (Ludwig, 2003). The zircon U–Pb age data are listed in Supplementary Table 1.

Hf isotope analyses were carried out using a New Wave-193 nm ArF-excimer laser-ablation system linked to a Neptune multiple-collector inductively coupled plasma mass spectrometer (LA-MC-ICP-MS). Instrumental parameters and data acquisition followed that described by Wu et al. (2006) and Geng et al. (2011). The analyses were conducted with a beam diameter of 50 μm, 8 Hz repetition rate with a laser power of 15 J/cm^2. External calibration was made by measuring zircon standard GJ-1 with the unknowns during the analyses to evaluate the reliability of the analytical data. The mean β_{Yb} value was applied for the isobaric interference correction of ^{176}Yb on ^{176}Hf in the same spot. The ratio of $^{176}Yb/^{172}Yb$ (0.5887) was also applied for the Yb correction. A decay constant for ^{176}Lu of 1.865×10^{-11} a^{-1} (Scherer et al., 2001), the present-day chondritic ratios of $^{176}Hf/^{177}Hf = 0.282772$ and $^{176}Lu/^{177}Hf = 0.0332$ (Blichert-Toft and Albarède, 1997) were adopted to calculate $\varepsilon_{Hf}(t)$ values. Single-stage Hf model ages (T_{DM1}) were calculated relative to the depleted mantle present-day value of $^{176}Hf/^{177}Hf = 0.28325$ (Nowell et al., 1998) and $^{176}Lu/^{177}Hf = 0.0384$ (Griffin et al., 2000). The zircon Hf isotopic compositions are listed in Supplementary Table 2.

5. Results

5.1. Age of the tuff sample from Sailajiazitage Group (SG)

Zircons in the sandy tuff sample from SG (2013TR06) range from 50 μm to 150 μm in length and have length to width ratios of 1–2. Most zircon crystals are euhedral or subhedral. Some zircons show zoning structure while others display homogenous inner structure (Fig. 6). Thirty-one analyses were carried out on 31 grains. Among them, one spot yields significantly discordant $^{206}Pb/^{238}U$ and $^{207}Pb/^{235}U$ ages and this spot was excluded for further discussions (Fig. 7a). Three spots on large-sized zircons yield older $^{206}Pb/^{238}U$ ages ranging from 1811 Ma to 2104 Ma (spot 23, 29, 31) and likely to be xenocrysts. The other 27 analyses could be divided into two groups. Group one analyses exhibit variable radiogenic lead loss but they defined a good discordia with an upper intercept age of 1401 ± 13 Ma ($N = 11$, MSWD = 0.31) (Fig. 7b). Group 1 zircons are relatively large and are likely xenocryts. Group two (G2, 16 spots) analyses were conducted on the zircons of smaller size (generally less than 80 μm, Fig. 6), and the results show variable U (171–555 ppm) and Th (82–343 ppm)

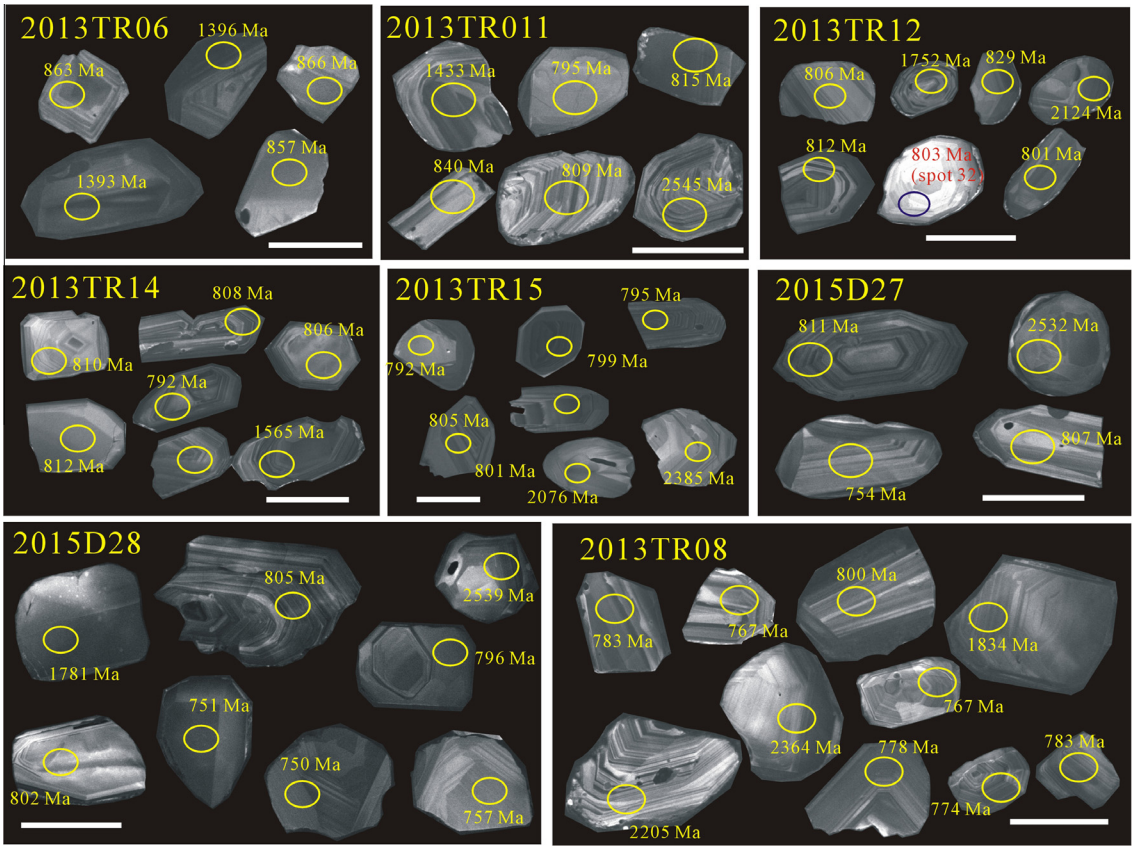

Fig. 6. Representative cathodoluminescence images of the zircons from the Neoproterozoic sequences in STT. The scale bar is 100 μm.

contents with Th/U ratios ranging from 0.50 to 0.99. G2 zircons yield broadly concordant $^{206}Pb/^{238}U$ and $^{207}Pb/^{235}U$ ages within analytical errors. One spot has a slight younger $^{206}Pb/^{238}U$ age for unknown reason while the other fifteen analyses yield a mean $^{206}Pb/^{238}U$ age of 857.1 ± 3.2 Ma (N = 15, MSWD = 3.2) (Fig. 7c). This age was interpreted as the deposition age of the SG volcanic-sedimentary sequence.

5.2. Ages of the detrital zircons from the Ailiankate Group (AG)

Zircons from the four clastic rock samples of the AG resemble each other. They range from 50 μm to 200 μm in length and have length to width ratios of 1–3. According to observations by the scanning electron microscope (SEM), some zircons from the clastic rocks are oval or round, indicating that their long-distance transportation (Fig. 8). In CL images, the detrital zircons show very different inner features (Fig. 6). Some of them exhibit oscillatory zoning, similar with that of the zircons crystallized from silicic magma, while others show homogenous or wide striped inner structure, sharing some features of the zircons crystallized from mafic magma.

Sixty analyses were carried on 60 zircon grains for sample 2013TR11. One zircon yields the oldest $^{206}Pb/^{207}Pb$ age of 3311 ± 11 Ma (spot 39) (Fig. 9a). Another two zircons yield broadly concordant Archean ages of ca.2880 Ma (spot 42) and ca.2550 Ma (spot 10). The other fifty-seven analyses have broadly concordant ages spanning from 800 Ma to 2400 Ma. A large population around at ca.800 Ma yield a mean $^{206}Pb/^{238}U$ age of 808 ± 3.2 Ma (N = 37, MSWD = 1.6) (Fig. 9b). We notice moderate peaks at ca.1400 Ma, 1800 Ma and 2000 Ma (insert of Fig. 9a and Supplementary Table 1). According to their CL images and Th and U contents, most grains are magmatic zircons (Fig. 6). Spot 24 (ca.1800 Ma) has very low Th/U ratios (0.04), indicative of a hydrothermal origin.

Fifty analyses were carried on 50 zircons for sample 2013TR12. Four spots yield Archean ages ranging from 2577 Ma to 2935 Ma (Fig. 9c, Supplementary Table 1). Other zircons yield similar ages with those of sample 2013TR11. Significant peaks at 800 Ma, 1400 Ma, 1800 Ma and 2400 Ma are observed (insert of Fig. 9c), and nearly a half of the total analyzed zircons yield a mean $^{206}Pb/^{238}U$ age of 805.7 ± 2.2 Ma (N = 22, MSWD = 0.74) (Fig. 9d). According to their Th and U contents (Th/U = 0.3–2.6 and mostly between 0.4 and 1.0) and CL image features, all the analyzed zircons are magmatic zircons.

Fifty-nine analyses were conducted on 59 zircons for sample 2013TR14. Most zircons yield ca.800 Ma concordant ages while some yield older ages ranging from 850 Ma to 2940 Ma (Fig. 9e). Among the zircons of Neoproterozoic ages, one spot has very low Th content (34 ppm) leading to low Th/U ratios (0.06), which is consistent with it very bright CL image and likely to be hydrothermal origin. The other zircons are magmatic origin in line with their CL image features and their Th/U ratios (mostly ranging from 0.3 to 1.1, see Supplementary Table 1). The Neoproterozoic zircons yield a mean $^{206}Pb/^{238}U$ age of 812.7 ± 1.7 Ma (N = 42, MSWD = 0.74) (Fig. 9f).

Thirty analyses were conducted on 30 zircon grains for sample 2013TR15. Similar with the scenario of sample 2013TR14, six spots yield broadly concordant ages ranging from 2076 Ma to 2424 Ma (Fig. 9g and Supplementary Table 1). Other zircons yield concordant and consistent $^{206}Pb/^{238}U$ and $^{207}Pb/^{235}U$ ages of ca.800 Ma with a mean $^{206}Pb/^{238}U$ age of 798.2 ± 2.1 Ma (N = 23, MSWD = 0.86) (Fig. 5h). One spot has very low U and Th contents and Th/U ratios (0.06), and yields significantly younger $^{206}Pb/^{238}U$ age (709 Ma). Its low Th/U and low U and Th contents may indicate that this rare younger zircon was likely affected by post-depositional metamorphism or metasomatism. We exclude this spot for further discussion.

As described above, the four samples collected from Ailiankate Group yield similar ages. We combine all the data in Fig. 10 that exhibits peaks at ca.800 Ma, 900–1000 Ma, ca.1400 M, ca.1800 Ma, ca.1900 Ma, ca.2400 Ma, ca.3000. These age peaks are consistent with the late Paleoproterozoic Columbia supercontinent and the late Mesoproterozoic to early Neoproterozoic Rodinia supercontinent assemblage and breakup events (Li et al., 2008; Zhao et al., 2002, 2011).

5.3. Ages of the detrital zircons from the tillite sequence (QG)

Zircons from sample 2015D27 range from 50 μm to 120 μm in length and have length to width ratios of 1–2. Most zircons are colorless and transparent and small amounts are light pinkish. They

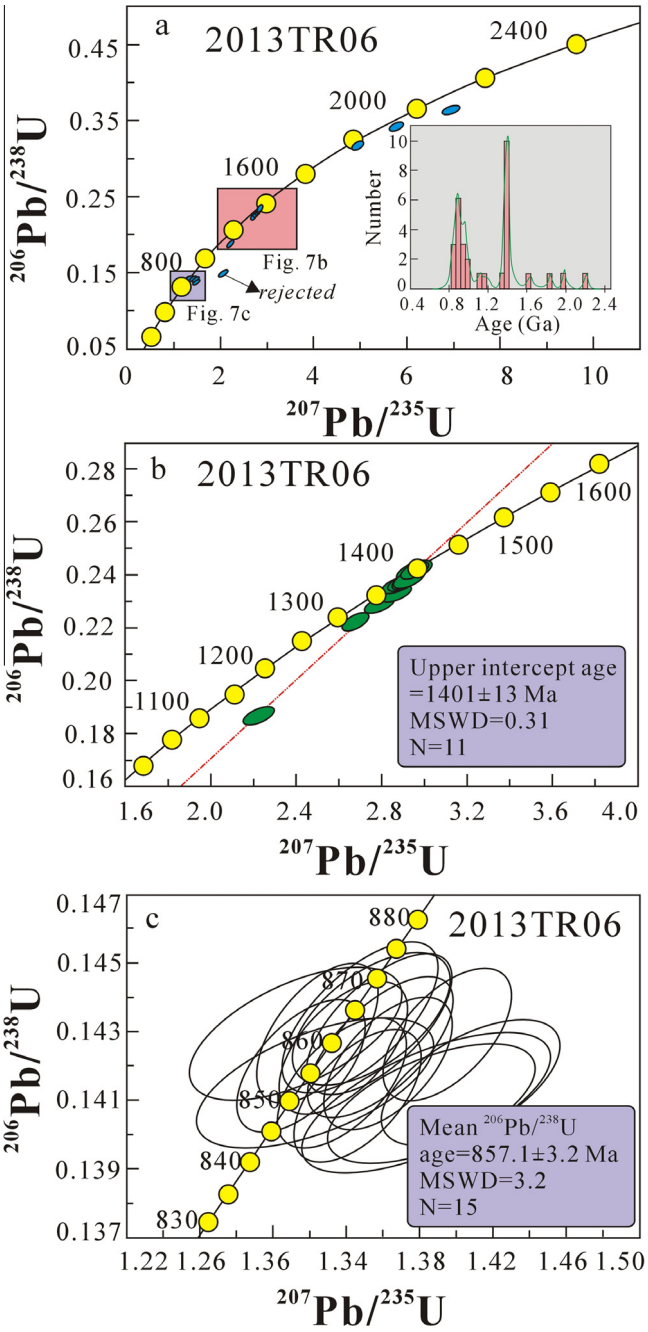

Fig. 7. Concordia of U–Pb zircon data for zircons from the sandy tuff sample of the Sailajiazitage Group (see details in the text).

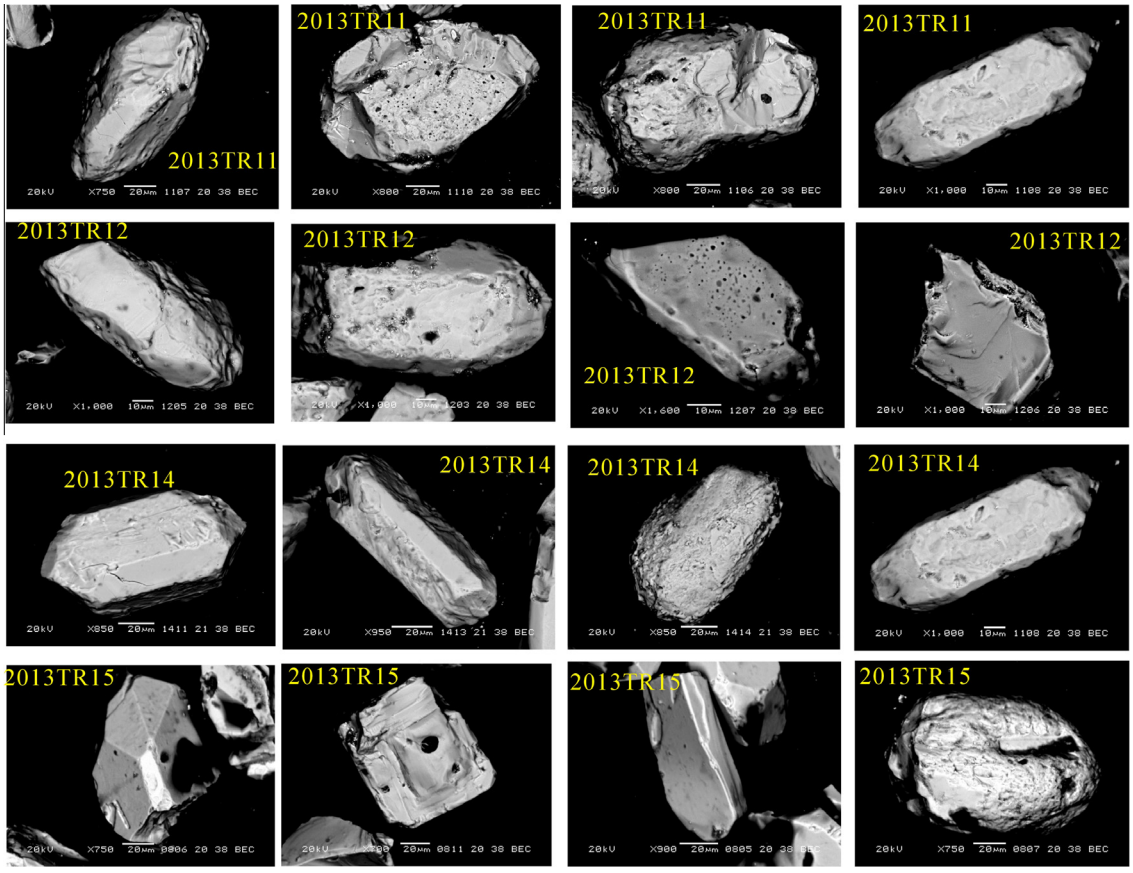

Fig. 8. Representative surface features of the zircons from AG samples observed under the scanning electron microscope (SEM).

are euhedral, subhedral or anhedral crystals, indicative of their variable distances of transportation. In CL images, some zircons show typical oscillatory and sector zoning while others show banded structure or homogeneous inner feature (Fig. 6). The distinct features of the zircons suggest their different sources. Sixty-four analyses were carried on 64 zircons and the results are presented in Supplementary Table 1. Among them, three spots yield significantly discordant $^{206}Pb/^{238}U$ and $^{207}Pb/^{235}U$ ages and they are excluded for further discussion. One spot (spot 35) yields $^{206}Pb/^{238}U$ age of 914 Ma. Seven analyses yield concordant older ages ranging from 2100 Ma to 2600 Ma (Fig. 11a). The other analyses could be divided into three groups. Group 1 zircons yield nearly concordant ages with a mean $^{206}Pb/^{238}U$ age of 1793 ± 13 Ma (N = 8, MSWD = 0.57) (Fig. 11b). Group 2 zircons yield concordant $^{206}Pb/^{238}U$ and $^{207}Pb/^{235}U$ ages, forming a tight cluster at ca.800 Ma with a mean $^{206}Pb/^{238}U$ age of 806.3 ± 3.4 Ma (N = 25, MSWD = 0.80) (Fig. 11c). Group 3 zircons form a tight cluster with a mean $^{206}Pb/^{238}U$ age of 748.0 ± 4.1 Ma (N = 21, MSWD = 1.3) (Fig. 11c). According to their high Th/U ratios (mostly between 0.4 and 1.0, Fig. 6 and Supplementary Table 1) and CL image features, these three groups of zircons are of magmatic origin.

Zircons from sample 2015D28 share most features with those of sample 2015D27 (Fig. 6). Sixty-one analyses were conducted on 61 zircon grains and among them, two spots deviate from the Concordia due to variable radiogenic lead loss. Eight analyses yield older ages spanning from 2133 Ma to 2656 Ma ($^{206}Pb/^{238}U$ ages) (Fig. 10d). Eight spots have consistent and almost concordant ages and yield a mean $^{206}Pb/^{238}U$ age of 1777.1 ± 6.4 Ma (N = 8, MSWD = 0.54) (insert of Fig. 11d). Due to slight radiogenic lead loss, these eight analyses defined a discordia with an intercept age of 1776 ± 13 Ma (N = 8, MSWD = 0.16) (insert of Fig. 11d). On the Concordia, the other analyses form two tight clusters with mean $^{206}Pb/^{238}U$ ages of 804.1 ± 4.7 Ma (N = 12, MSWD = 1.2) and 752.9 ± 3.1 Ma (N = 29, MSWD = 2.9), respectively (Fig. 11e). Thus, the results from sample 2015D27 and 2015D28 are comparable to each other.

Zircons from sample 2013TR08 range from 50 μm to 120 μm in length with length/width ratios from 1 to 3. Most zircons are transparent and colorless and some are light pink. They are euhedral, subhedral or anhedral. Some anhedral grains show oval shape due to long distance transportation. In CL images, oscillatory and sector zoning, banded structure and homogeneous structure are observed (Fig. 6), indicating their distinct origin. Seventy analyses were carried on 70 zircons and yield ages spanning from 750 Ma to 2620 Ma (Supplementary Table 1). Among them, four zircons yield Archean ages (spot 1, 34, 59, 62) and six yield Paleoproterozoic ages (spot 9, 15, 33, 47, 68, 69) (Fig. 11f). Zircons of late Paleoproterozoic ages could be divided into two main groups. Group 1 zircons yield almost concordant ages with a mean $^{206}Pb/^{238}U$ age of 1970 ± 16 Ma (N = 4, MSWD = 3.2) and G2 zircons yield with a mean $^{206}Pb/^{238}U$ age of 1814 ± 13 Ma (N = 8, MSWD = 9.1) (Fig. 11g). The dominant zircon population of this sample yield Neoproterozoic ages ranging from 740 Ma to 810 Ma and on the Concordia, forming a tight cluster at ca.780 Ma. Taking several spots of variable radiogenic lead loss into account, they yield an intercept age of 775.1 ± 4.6 Ma (MSWD = 13). Nevertheless, the youngest four zircons yield a mean $^{206}Pb/^{238}U$ age of 751 ± 6 Ma (N = 4, MSWD = 3.2) (Fig. 11h).

When we combine these three samples together, the detrital zircons from the tillite sequence exhibit 3 strong peaks at ca.745 Ma, 800 Ma, 1800 Ma and 2 weak peaks at 2250 Ma and 2500 Ma (Fig. 12). There is obvious hiatus between 1000 Ma and 1800 Ma.

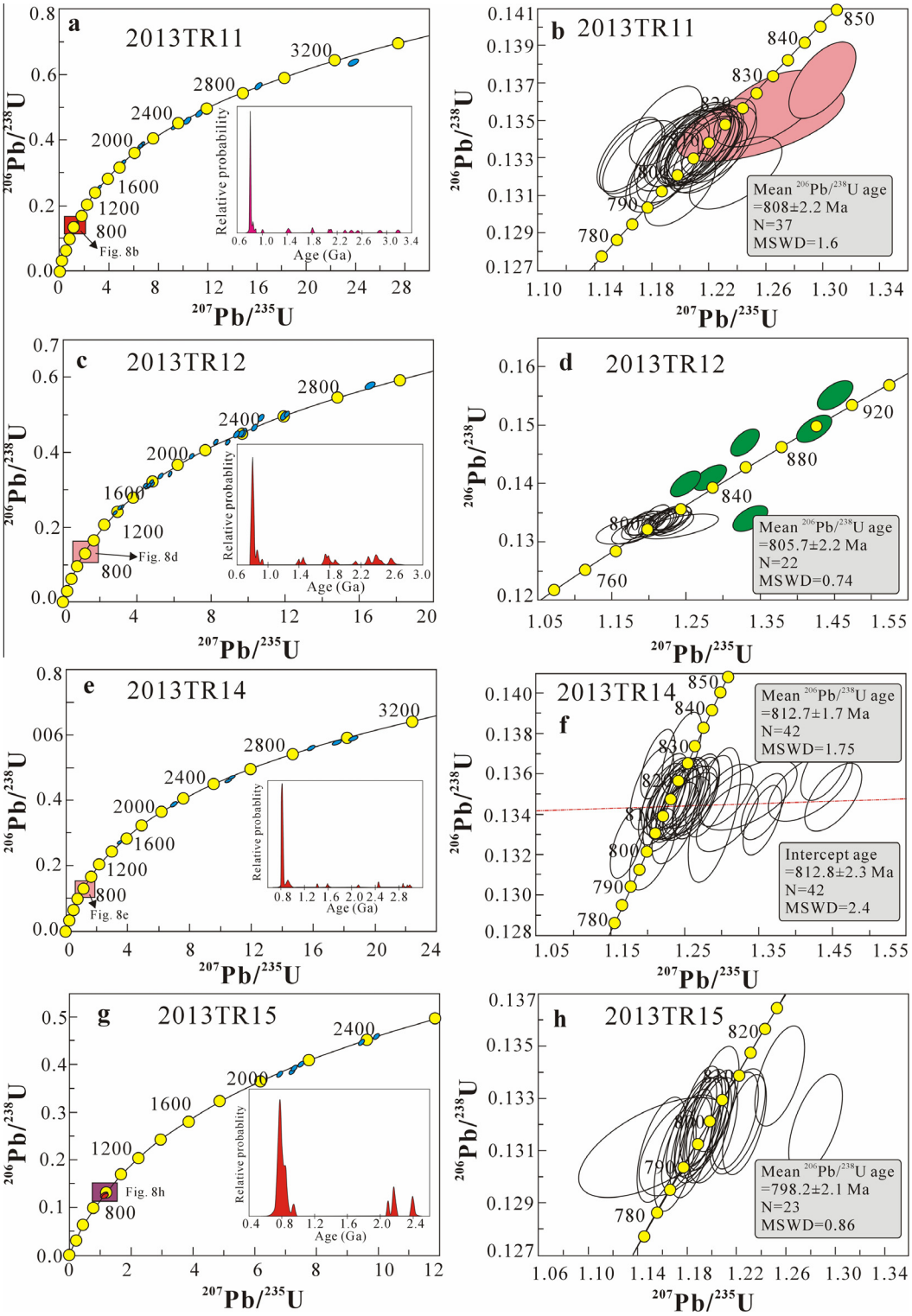

Fig. 9. Concordia of the detrital zircons U–Pb data of the clastic rock samples collected from AG (see details in the text).

5.4. Zircon Hf isotope compositions

In this study, six samples were analyzed for their Lu–Hf isotope compositions and the results are listed in Supplementary Table 2 (calculation formulas and the ages used in calculations are listed at the footnotes of this table).

The ca.857 Ma zircons from the SG tuff sample have a large range of $\varepsilon Hf(t)$ values ranging from −2 to 9.6, possibly due to variable involvement of the magma derived from a depleted mantle source (see following discussions). In this sample, detrital zircons of ca.1.4 Ga have $\varepsilon Hf(t)$ values between −1.8 and 2.4, similar to the zircons from 1.4 Ga Azibailedi A-type granite (Huang et al., 2012; Ye et al., 2016), indicating that some detritus of this sandy tuff sample may be derived from this granitic pluton. The $\varepsilon Hf(t)$ values of the 820–800 Ma detrital zircons from the AG and the QG range from −20 to 6. Other detrital zircons with ages

older than 1.4 Ga from all of the six samples have wide range of εHf (t) values, and some zircons of 2.3–2.4 Ga were most likely derived from the Heluositan complex according to their overlapping εHf(t) values (rectangle region in Fig. 13a).

In the age vs. εHf(t) diagram (Fig. 13a, the reported Heluositan complex and the 1.4 Ga Azibailedi granite are also included), their evolution trend significantly deviates from that of the Mesoarchean basement of the North China Craton and the Yangtze Craton. Significant positive deviation at ca.800 Ma and ca.1400 Ma indicates the contribution of the juvenile crust. T^{C}_{DM} of the detrital zircons vary from 1.2 Ga to 4.5 Ga with peaks at 2.5 Ga and 3.6–3.7 Ga (Fig. 13b).

6. Discussion

6.1. Tectonic setting of the SG volcanic-clastic sequence

The youngest detrital zircon ages represent the maximum depositional ages. The youngest zircon age (857 Ma) of the sandy tuff sample from SG argues that the volcanic-clastic sedimentary sequence likely deposited at the middle Neoproterozoic rather than Mesoproterozoic, as the lowest Neoproterozoic package in southwestern Tarim terrane. A concordant zircon SHRIMP U–Pb age of 830 Ma from the rhyolite of SG has been obtained by Mr. Y.Z. Zheng from the No. 11 Geological Team of Xinjiang BGMR (personal communications). Thus, we can conclude that the deposition age of the SG is between 860 and 830 Ma. As we have described above, bimodal volcanic rocks (basalt–rhyolite) account for about half of the total thickness of the SG and they can be used as indicator for their tectonic background. Elemental compositions of the bimodal volcanic rocks from this group show typical intraplate features (Guo et al., 2004; Yuan et al., 2004). Zircon Hf isotope compositions indicate variable involvements of the depleted mantle derived magma in the petrogenesis of the volcanic rocks. In combination with the low maturity of the clastic rocks and the age spectra of the tuff sample (insert of Fig. 7a) (Cawood et al., 2012), we suggest that the SG was most likely deposited at a back-arc basin or a rift basin.

6.2. Age and tectonic setting of the AG

As described above, the four clastic samples from AG yield similar ages (Fig. 9). According to the shapes of the detrital zircons (Fig. 8), most of them are euhedral crystals, indicative of short distance transportation. Their age spectra show features of the foreland basin, such as the Cordillera, far away from the rift basin. Generally, foreland basin sample includes detritus with ages close to the deposition of the sample, reflecting input from syn-collisional as well as convergent plate magmatism, along with significant input from older sources (Cawood et al., 2012). In line with field observations, the AG underwent lower greenschist facies metamorphism and strong deformation, and the undeformed and unmetamorphosed Neoproterozoic carbonate–clastic–tillite sequence unconformably overlies the AG (Xinjiang, 1993, see following discussions). Thus, we suggest that the deposition age of the AG was slightly younger than 810–800 Ma.

6.3. Age and tectonic setting of the Neoproterozoic tillite sequence (QG)

The depositional age of the carbonate–clastic–tillite sequence (SLG and QG) and the glacial epoch comparison with that of the tillite in the Quruqtagh and in Aksu areas at the northern margin of Tarim remain unclear. The age spectra of the two sandstone samples collected at the bottom and within the BF tillite are comparable to each other. The juvenile groups yield ca.750 Ma concordant ages, which is nearly concurrent with the age of the volcanic rocks occurring at the lowest unit of the Beiyixi Group in the Quruqtagh (Xu et al., 2009). The youngest four zircons collected from the conglomerate-bearing sandstone sample (2013TR08) of the KXF, yield a mean age of 751 Ma. The age spectra of the three samples shares some features of passive margin such as the western Australia (Cawood et al., 2012) with two relatively juvenile peaks at ca.745 Ma and 800 Ma (Fig. 12). The QG tillite sequence lacks any significant deformation and metamorphism, similar to the scenario of the Quruqtagh Group and tillite sequence in the Aksu area (see Fig. 2 of Xu et al. (2009) and Fig. 5 of Turner (2010), Fig. 4), which is inconsistent with those of the convergent and collisional basins, because basins lying along the extensional and trailing edge settings (rift basins and passive margins) generally lack a component of syn-depositional magmatic activities and are dominated by input from older sources (Cawood et al., 2012). Nevertheless, as middle to late Neoproterozoic igneous activities, possibly related to the Rodinia superplume (Li et al., 2008, 2009), have been well documented in Tarim (Zhang et al., 2006, 2007a, 2012b; Xu et al., 2005, 2009; Shu et al., 2011), the large populations of 750 Ma and 800 Ma zircons were most likely sourced from these nearby and recently emplaced/erupted igneous rocks.

According to micropaleontology studies and stratigraphic correlation, some geologists suggested that the BF tillite and the YTF tillite could be equivalent with the Beiyixi and Altungol–Tereeken tillite, respectively (Gao et al., 1980, 1985; Ma et al., 1989, 1991; Wang, 2000), whereas Tong et al. (2013) correlated the BF and YTF tillites with the Tereeken and Hankalchough tillites, respectively. The detrital zircon ages obtained in this study favor the first correlation scheme though solid evidence for the ages of the two phases of glaciation in southern Tarim are still lacking (Fig. 4).

Previous studies demonstrated that the Neoproterozoic cover sequences in Tarim show significant affinities with those of the Yangtze (Wang et al., 2004; Lu et al., 2008; Gao et al., 2013a,b). We also noticed that the age spectra of the QG share some features with those of the Banxi Group and Liantuo Formation in South China (Gao and Zhang, 2009; Lan et al., 2015). Nevertheless, due to a lack of strong evidence, the comparison between the glaciations in Yangtze and Tarim remains unsolved.

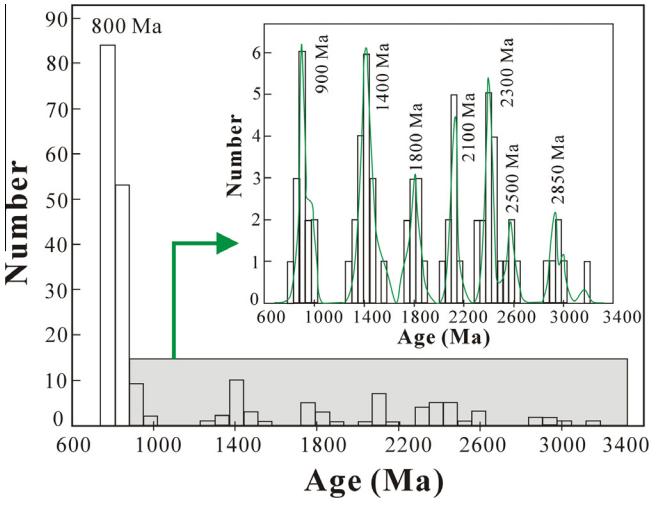

Fig. 10. Histograms of $^{206}Pb/^{238}U$ ages of the detrital zircon from the clastic rocks of the AG (sample 2013TR11, 2013TR12, 2013TR14, 2013TR15).

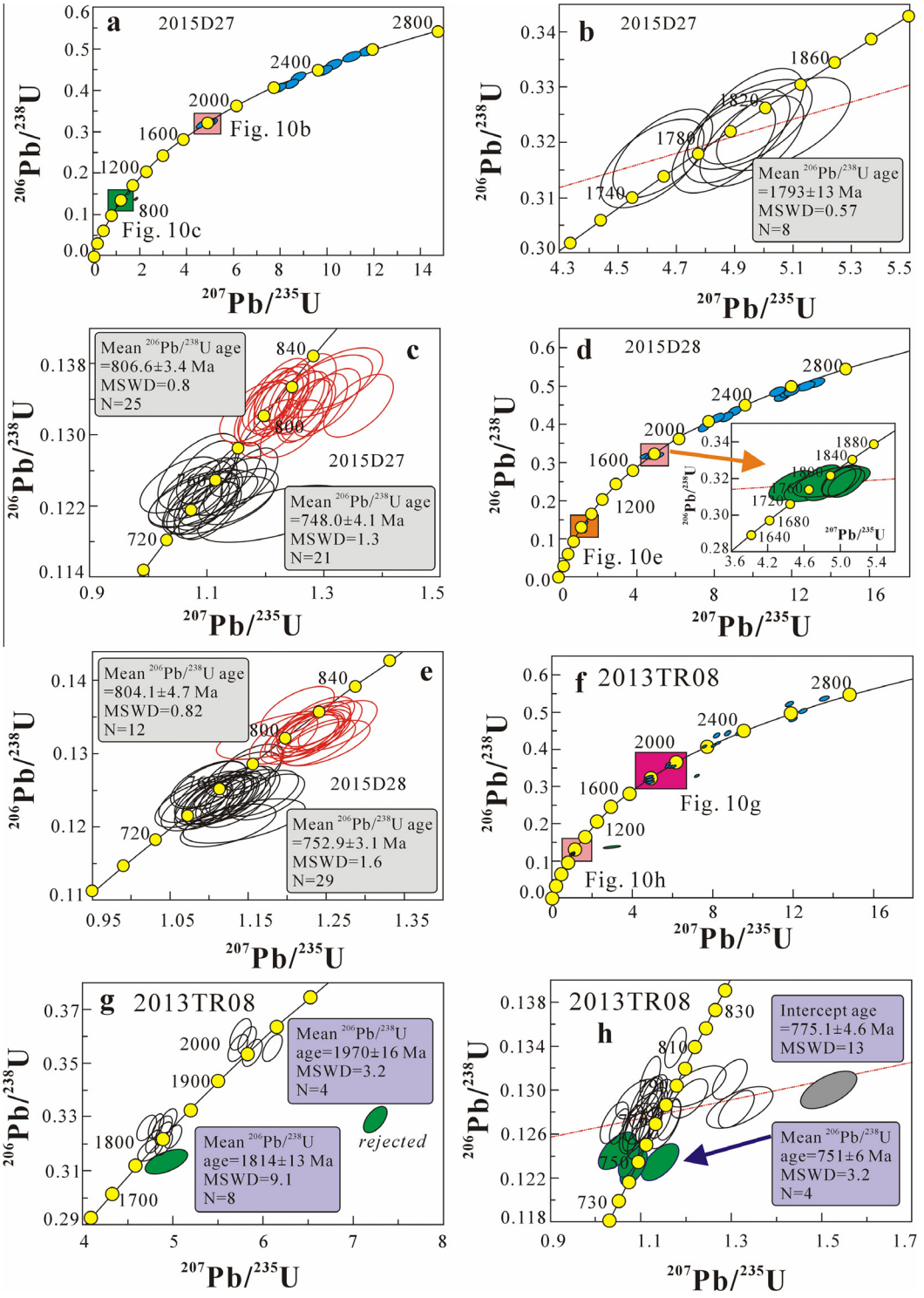

Fig. 11. Concordia of the detrital zircons U–Pb data of the clastic rock samples collected from QG (see details in the text).

6.4. Neoproterozoic sedimentary chronosequence

Wang et al. (2015) suggested that the AG deposited after 630 Ma according to detrital zircon U–Pb age dating. We checked their data and found that most analyzed detrital zircons yielded 830–800 Ma. Among more than one hundred analyses only two spots yield juvenile ages. Although the youngest detrital zircon ages represent the maximum depositional ages, these two juvenile ages need to be double checked if they were affected by post-depositional metamorphism or metasomatism. Both AG and SG underwent greenschist facies metamorphism and tight folding deformation while the Neoproterozoic carbonate–clastic–tillite sequences exhibit no metamorphism and no deformation (Ma et al., 1989, 1991; Wang et al., 2004). If the AG deposition age is younger than 630 Ma (Wang et al., 2015), then the two phases of glaciation in QG could not correlate to any phase of the glaciation in the Quruqtagh in north Tarim, because more than 2000 m carbonate–clastic layer between the AG and QG (i.e., the SLG, Wang

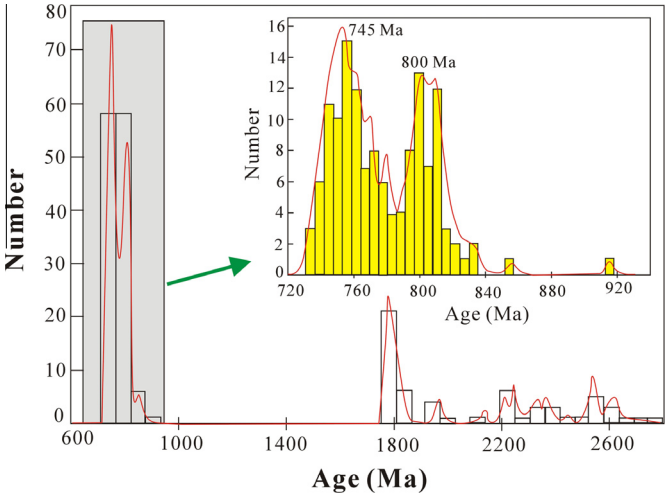

Fig. 12. Histograms of $^{206}Pb/^{238}U$ ages of the detrital zircon from the clastic rocks of the QG (sample 2015D27, 2015D28, 2013TR08).

et al. (2004)), as well as the ca.200 m silicolite at the bottom of QG, needs more than 50 Ma for their deposition according to the average sedimentation rate at a stable environment (0.03–0.05 cm/y, Park et al. (2000), Li et al. (2009)). Thus, the deposition age of the two phases of tillite in QG would be younger than 580 Ma, which is obviously unlikely, as the first phase of glaciation in northern Tarim has been constrained as 740–725 Ma (Xu et al., 2009). On the other hand, the ca.492 Ma massive-structure and fresh granite sheet in AG give the lower limit of the metamorphism and deformation of AG. Thus, the metamorphism and deformation could be constrained between 630 Ma and 490 Ma. No orogenic events have ever been documented along the southwestern Tarim.

We also notice that Wang et al. (2014, 2015) used single or very few most juvenile detrital zircons ages to constrain the deposition ages of the BCF and the QG. For the same reasons described above, we suggest that their constraints may not be robust.

Synthesizing the detrital zircon U–Pb ages, rock association, metamorphic and deformation features and the contact relations of the different members of the Neoproterozoic sedimentary packages, we construct a possible chronosequence of the Neoproterozoic in STT, i.e., in an ascending order from early to late, the 860–830 Ma SG, the 820–800 Ma AG and the SLG-QG later than 760 Ma (Fig. 14).

6.5. Implications of the zircon Hf isotope compositions

According to systematic zircon Hf isotope analyses, we noticed significant positive deviations of the 1400 Ma and 820–800 Ma zircons (Fig. 13). The 820–800 Ma deviation was highly likely due to the effects of the Rodinia superplume as demonstrated by many previous studies (Zhang et al., 2006, 2009; Li et al., 2008, and references therein).

The histogram of T^{C}_{DM} of the detrital zircons and the zircons from the 2.3–2.4 Ga Heluositan complex shows that the continental crust growth mainly took place during 2.3–4.0 Ga with two obvious peaks at 2.5–2.7 Ga and 3.6–3.8 Ga (Fig. 13b). However, we must point out that the Neoproterozoic zircons could source from the Australia continent and/or other neighboring terranes in Tarim (Zhang et al., 2014a; Ye et al., 2016), they could not be used to decipher the continental growth of the STT.

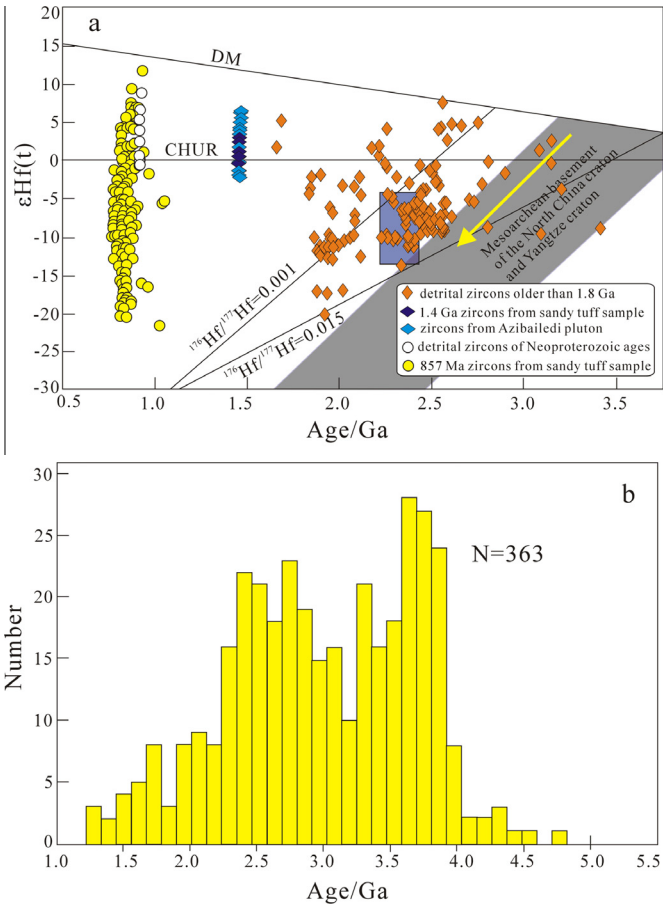

Fig. 13. Crystallization age vs. $\varepsilon Hf(t)$ diagram and histogram of the T^{C}_{DM}. The square marks the range of the $\varepsilon Hf(t)$ values of the zircons from Heluositan complex (see details in the text).

6.6. Neoproterozoic tectonic evolution of the southwestern Tarim

In line with the hornblende and biotite $^{39}Ar/^{40}Ar$ plateau ages of the KG, Zhang et al. (2003a,b) suggested that the STT amalgamated with north Australia at ca.1.0 Ga (Fig. 14a and b) (Huang et al., 2005; Li et al., 2008). Based on the geochronological data of the samples collected from the drilling holes in central Tarim and the aeromagnetic anomaly belt cross the central Tarim in EW direction (Wu et al., 2012), Xu et al. (2013a,b) argued that the STT and the NTT unified together along the central Tarim suture zone at the middle Neoproterozoic (ca.820 Ma). If this model is favorable, it could well interpret the Neoproterozoic basins evolution in STT.

After the STT amalgamated with Australia at ca.1.0 Ga, the south dipping subduction along the central Tarim led to the nascent of the back-arc basin in STT. This back-arc basin, as represented by SG volcanic-sedimentary sequence, possibly initiated at ca.860 Ma or a little earlier and lasted at least to ca.830 Ma (Fig. 14c). As the NTT and STT amalgamated together along the central Tarim suture zone, at this time in STT, transformation from extension to compression induced the formation of the foreland basin on the previous back-arc sequence (i.e., the AG clastic rocks) (Fig. 14d). At the same time, the Aksu Group volcanic-clastic rocks deposited at a forearc basin (Fig. 14d, Zhang et al., 2014b). The closing, low greenschist facies metamorphism and folding of the foreland basin package (AG) most likely took place at ca.760–750 Ma, geodynamically related to the blueschist facies metamorphism of the Aksu Group in the northern margin of the Tarim (Liou et al., 1996; Yong et al., 2013; Zhang et al., 2014b).

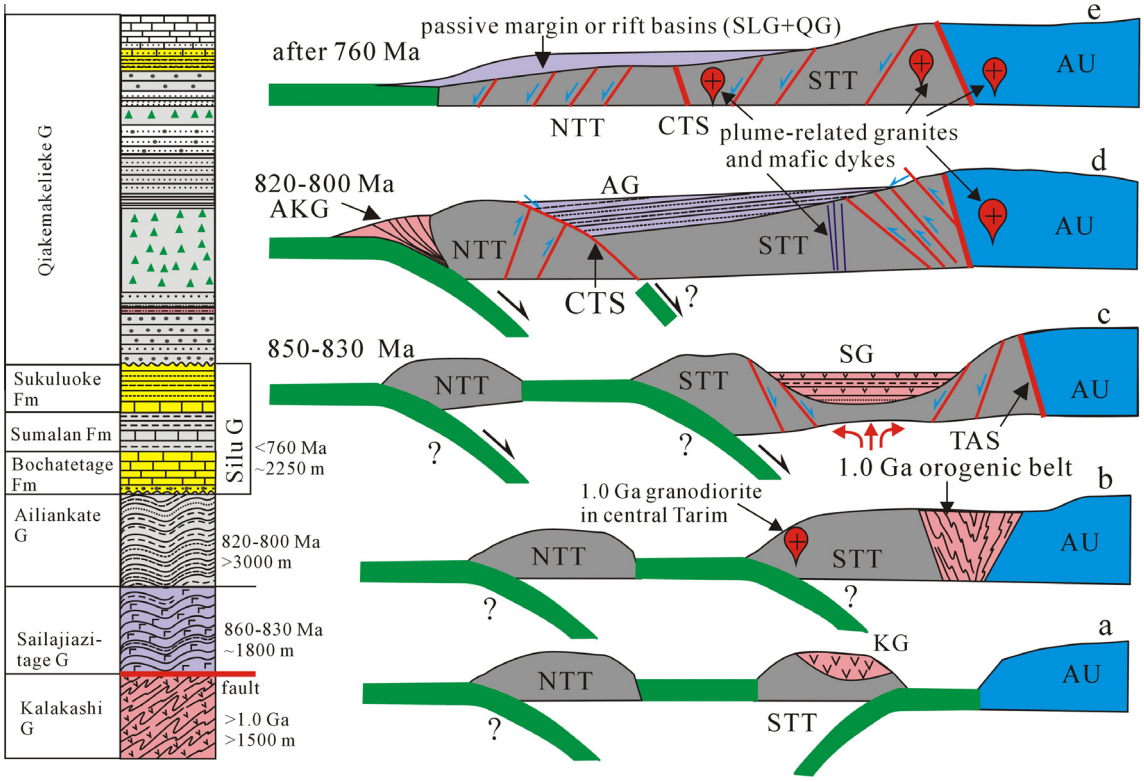

Fig. 14. A schematic diagram to illustrate the relationship between the evolution of the late Mesoproterozoic–Neoproterozoic sedimentary basins and tectonic evolution process along the southwestern margin of the Tarim. The main four tectonic evolution stages from early to late include stage 1, the late-Mesoproterozoic northward subduction along the southern margin of STT induced the formation of the Kalakashi Group (KG) volcanic arc and then STT and Australia assembled together at ca.1.0 Ga according to the 1.0 Ga metamorphism of the KG (a, b); stage 2, the southward subduction along the northern margin of the STT led to the formation of the back-arc basin during 860–830 Ma (c); stage 3, the foreland basin developed on the back-arc basin sedimentary package due to the suture of the STT and the NTT along the central belt of the Tarim (see Xu et al. (2013a,b)) (d) and stage 4, the accretion of the Aksu blueschist terrane along the north margin of the NTT, led to low greenschist-facies metamorphism and deformation of the foreland basin sedimentary sequence and then after 760 Ma, on the folded back-arc basin and foreland basin sedimentary packages, deposited the passive/rift basin cover sequences (e). The left stratigraphic column showing the Neoproterozoic sedimentary chronosequence, the thickness is not by scale. Abbreviations: KG-Kalakashi Group, SG- Sailajiazitage Group, AG-Ailiankate Group, AKS-Aksu Group, SLG-Silu Group, QG-Qiakemakelieke Group, AU-Australia, STT-South Tarim terrane, NTT-north Tarim terrane, CTS-central Tarim suture zone, TAS-Tarim–Australia suture zone.

After the formation of the uniform basement of the Tarim at ca.760 Ma, passive margin and/or rift basins developed, and this tectonic setting continued, at least, till Cambrian, forming the middle Neoproterozoic to Cambrian unmetamorphosed and undeformed cover packages of the Tarim (i.e., the SLG and QG, Fig. 14e), consistent with the breakup of the Rodinia supercontinent (Li et al., 2008 and references therein).

7. Conclusions

Field observations, detrital zircon U–Pb ages and Hf isotope compositions and a comprehensive synthesis on the regional geology lead us to draw the following main conclusions:

(1) The SG volcanic-sedimentary sequence deposited during 850–830 Ma, the AG clastic rocks of lower greenschist facies metamorphism and intensive deformation deposited during 820–800 Ma, and the unmetamorphosed and undeformed late Neoproterozoic calstic–tillite sequence deposited after 760 Ma. The BF glaciation and the YTF glaciation in southwestern Tarim could be equivalent to the Beiyixi glaciation and the Altungol–Tereeken glaciation, respectively.
(2) Rock association coupled with geochemistry of the SG volcanic rocks indicates the SG deposited at a back arc basin. Detrital zircon age spectra and its metamorphism and deformation features suggest that the AG clastic sequence most likely deposited at a foreland basin after the closing of the back-arc basin in southwestern Tarim. The middle to late Neoproterozoic clastic–tillite sequences deposited at a passive marginal and/or rift basins.
(3) Zircon Hf isotope compositions of the detrital zircons suggest that the Rodinia plume could have effects on the Neoproterozoic igneous activities.
(4) The Neoproterozoic evolution process of the southwestern Tarim demonstrated that the Neoproterozoic assemblage of the Tarim basement could have lasted till 760 Ma and its Pre-Nanhuaian basement is composed by several independent continental terranes.

Acknowledgements

We sincerely thank Mr. Zheng Yuzhuang for his help with the field work and supplying the 1/50,000 geological maps. We appreciate the assistances of Hong-Ying Zhou in LA-ICP-MS dating, Zhang Jian and Zhang Yong-Qing for their help with zircon Lu–Hf isotope analyses. We are grateful to Jian Wang and an anonymous reviewer for their constructive journal reviews that considerably improved the quality of this paper. This study is financially supported by the National 305 Project of China (2015BAB05B01-01), National Science Foundation of China (41172175) and National Science and Technology Major Project (2016ZX05004001-005).

Appendix A. Supplementary data

Supplementary data associated with this article can be found, in the online version, at http://dx.doi.org/10.1016/j.precamres.2016.04.011.

References

Andersen, T., 2002. Correction of common lead in U–Pb analyses that do not report ^{204}Pb. Chem. Geol. 192, 59–79.

Blichert-Toft, J., Albarède, F., 1997. The Lu–Hf isotope geochemistry of chondrites and the evolution of the mantle–crust system. Earth Planet. Sci. Lett. 148, 243–258.

Cawood, P.A., Hawkesworth, C.J., Dhuime, B., 2012. Detrital zircon record and tectonic setting. Geology 40, 875–878.

Cawood, P.A., Nemchin, A.A., Strachan, R.A., 2007a. Provenance record of Laurentian passive-margin strata in the northern Caledonides: implications for paleodrainage and paleogeography. Geol. Soc. Am. Bull. 119, 993–1003.

Cawood, P.A., Nemchin, A.A., Strachan, R.A., Prave, A.R., Krabbendam, M., 2007b. Sedimentary basin and detrital zircon record along East Laurentia and Baltica during assembly and breakup of Rodinia. J. Geol. Soc. 164, 257–275.

Condie, K.C., Belousova, E., Griffin, W.L., Sircombe, K.N., 2009a. Granitoid events in space and time: constraints from igneous and detrital zircon age spectra. Gondwana Res. 15, 228–242.

Condie, K.C., O'Neill, C., Aster, R.C., 2009b. Evidence and implications for a widespread magmatic shutdown for 250 My on Earth. Earth Planet. Sci. Lett. 282, 294–298.

Feng, B.Z., Zhou, Y.W., Chi, S.F., 1995. Presinian geology, precious and nonferrous mental deposits in Quruqtagh area. Xinjiang Uygur Autonomous Region. Geological Publishing House, Beijing, China, pp. 23–125 (in Chinese).

Gao, L.Z., Ding, X.Z., Yin, C.Y., Zhang, C.H., Ettensohn, F.R., 2013a. Qingbaikouan and Cryogenian in South China: constraints by SHRIMP zircon U–Pb dating. Acta Geol. Sin. 87, 1540–1553.

Gao, L.Z., Lu, J.P., Ding, X.Z., Wang, H.R., Liu, Y.X., Li, J., 2013b. Zircon U–Pb dating of Neoproterozoic tuff in South Guangxi and its implications for stratigraphic correlation. Geol. China 40, 1443–1452 (in Chinese with English abstract).

Gao, W., Zhang, C.H., 2009. Zircon SHRIMP U–Pb ages of the Huangling granite and the tuff beds from Liantuo Formation in the Three Gorges area of Yangtze River, China and its geological significance. Geol. Bull. China 28, 45–50 (in Chinese with English abstract).

Gao, Z.J., Chen, K.Q., 2003. The Nanhua system of Xinjiang and some geological issues of Nanhua system in China. Geol. Surv. Res. 26, 8–14 (in Chinese with English abstract).

Gao, Z.J., Wu, S.Z., Li, Y.A., Qian, J.X., 1980. Sinian–Cambrian in Aksu–Keping area, Xinjiang. Chin. Sci. Bull. 12, 741–743 (in Chinese).

Gao, Z.J., Wang, W.Y., Peng, W.C., Li, Y.A., Xiao, B., 1985. Sinian in Xinjiang Uygur Autonomous Region. Xinjiang People Publishing House, Urumqi, pp. 35–98 (in Chinese).

Geng, J.Z., Li, H.K., Zhang, J., Zhang, Y.Q., 2011. Zircon Hf isotope analysis by means of LA–MC–ICP–MS. Geol. Bull. China 30, 1508–1513 (in Chinese with English abstract).

Ge, R.F., Zhu, W.B., Wu, H.L., He, J.W., Zheng, B., 2013a. Zircon U–Pb ages and Lu–Hf isotopes of Paleoproterozoic metasedimentary rocks in the Korla complex, NW China: implications for metamorphic zircon formation and geological evolution of the Tarim Craton. Precambrian Res. 231, 1–18.

Ge, R.F., Zhu, W.B., Wu, L., Zheng, B.H., He, J.W., 2013b. Timing and mechanisms of multiple episodes of migmatization in the Korla complex, northern Tarim Craton, NW China: constraints from zircon U–Pb–Lu–Hf isotopes and implications for crustal growth. Precambrian Res. 231, 136–156.

Gehrels, G., 2014. Detrital zircon U–Pb geochronology applied to tectonics. Annu. Rev. Earth Planet. Sci. 42, 127–149.

Griffin, W.L., Pearson, N.J., Belousova, E., Jackson, S.E., Van Achterbergh, E., O'Reilly, S.Y., Shee, S.R., 2000. The Hf isotope composition of cratonic mantle: LAM–MC–ICPMS analysis of zircon megacrysts in kimberlites. Geochim. Cosmochim. Acta 64, 133–147.

Grove, M., Bebout, G.E., Jacobson, C.E., Barth, A.P., Kimbrough, D.L., King, R.L., Zou, H. B., Lovera, O.M., Mahoney, B.J., Gehrels, G.E., 2008a. The Catalina schist: evidence for middle cretaceous subduction erosion of southwestern North America. Geol. Soc. Am. Spec. Pap. 436, 335–361.

Grove, M., Gehrels, G.E., Cotkin, S.J., Wright, J.E., Zou, H.B., 2008b. Non-Laurentian cratonal provenance of late Ordovician eastern Klamath blueschists and a link to the Alexander terrane. Geol. Soc. Am. Spec. Pap. 438, 223–250.

Guo, K.Y., Zhang, C.L., Shen, J.L., Ye, H.M., Wang, A.G., Li, C.H., 2004. Geochemistry of the Statherian volcanic rocks in the western Kunlun Mountains. Geol. Bull. China 23, 130–135 (in Chinese with English abstract).

Guo, Z.J., Yin, A., Robinson, A., Jia, C.Z., 2005. Geochronology and geochemistry of deep-drill-core samples from the basement of the central Tarim basin. J. Asian Earth Sci. 25, 45–56.

Guo, X.C., Zheng, Y.Z., Gao, J., Zhu, Z.X., 2013. Determination and geological significance of the Mesoarchean Craton in western Kunlun Mountains, Xinjiang, China. Geol. Rev. 59, 401–412.

Hawkesworth, C., Dhuime, B., Pietranik, A., Cawood, P., Kemp, T., Storey, C., 2010. The generation and evolution of the continental crust. J. Geol. Soc. 167, 229–248.

He, Z.Y., Zhang, Z.M., Zong, K.Q., Wang, W., Santosh, M., 2012. Neoproterozoic granulites from the northeastern margin of the Tarim Craton: petrology, zircon U–Pb ages and implications for the Rodinia assembly. Precambrian Res. 212–213, 21–33.

Huang, B.C., Xu, B., Zhang, C.X., Li, Y.A., Zhu, R.X., 2005. Paleomagnetism of the Baiyisi volcanic rocks (ca.740 Ma) of Tarim, Northwest China: a continental fragment of Neoproterozoic Western Australia? Precambrian Res. 142, 83–92.

Huang, J.G., Yang, R.D., Yang, J., Cui, C.L., Hou, L.J., 2012. Mesoproterozoic magmatic activities and its geological significance in Kusilafu area of the northern margin of western Kunlun. Chin. J. Geol. 47, 867–885.

Hou, K.J., Li, Y.H., Tian, Y.R., 2009. In situ U–Pb zircon dating using laser ablation multi ion counting-ICP-MS. Mineral Deposit 28, 481–492 (in Chinese with English abstract).

Jackson, S.E., Pearson, N.J., Griffin, W.L., Belousova, E.A., 2004. The application of laser ablation-inductively coupled plasma-mass spectrometry (LA-ICP-MS) to in situ U–Pb zircon geochronology. Chem. Geol. 211, 47–69.

Kemp, A.I.S., Hawkesworth, C.J., Paterson, B.A., Kinny, P.D., 2006. Episodic growth of the Gondwana supercontinent from hafnium and oxygen isotopes in zircon. Nature 439, 580–583.

Lan, Z.W., Li, X.H., Zhu, M.Y., Zhang, Q.R., Li, Q.L., 2015. Revisiting the Liantuo formation in yangtze block, South China: SIMS U–Pb zircon age constraints and regional and global significance. Precambrian Res. 263, 123–141.

Liu, Y.S., Hu, Z.C., Gao, S., Gunther, D., Xu, J., Gao, C., Chen, H., 2008. In situ analysis of major and trace elements of anhydrous minerals by LA-ICP-MS without applying an internal standard. Chem. Geol. 257, 34–43.

Li, Z.X., Bogdanova, S.V., Collins, A.S., Davidson, A., Waele, B.De., Ernst, R.E., Fitzsimons, I.C.W., Fuck, R.A., Gladkochub, D.P., Jacobs, J., Karlstrom, K.E., Lu, S., Natapov, L.M., Pease, V., Pisarevsky, S.A., Thrane, K., Vernikovsky, V., 2008. Assembly, configuration, and break-up history of Rodinia: a synthesis. Precambrian Res. 160, 179–210.

Liou, J.G., Graham, S.A., Maruyama, S., Zhang, R.Y., 1996. Characteristics and tectonic significance of the late Proterozoic Aksu blueschists and diabasic dikes northwest Xinjiang, China. Int. Geol. Rev. 38, 228–244.

Li, X.H., Li, Z.X., Li, W.X., 2014. Detrital zircon U–Pb age and Hf isotope constrains on the generation and reworking of Precambrian continental crust in the Cathaysia Block, South China: a synthesis. Gondwana Res. 25, 1202–1215.

Li, Y.J., Song, W.J., Wu, G.Y., Wang, Y.F., Li, Y.P., Zheng, D.M., 2005. Jinning granodiorite and diorite deeply concealed in the central Tarim Basin. Sci. China 48, 2061–2068 (D-series).

Li, J., Hu, B.Q., Dou, Y.G., Zhao, J.T., Li, G.G., 2009. Modern sedimentation rate budget and supply of the muddy deposits in the East China Seas. Geol. Rev. 58, 745–756 (in Chinese with English abstract).

Long, X.P., Yuan, C., Sun, M., Zhao, G.C., Xiao, W.J., Wang, Y.J., Yang, Y.H., Hu, A.Q., 2010. Archean crustal evolution of the northern Tarim Craton, NW China: zircon U–Pb and Hf isotopic constraints. Precambrian Res. 180, 272–284.

Long, X.P., Yuan, C., Sun, M., Kroner, A., Zhao, G.C., Wilde, S., Hu, A.Q., 2011. Reworking of the Tarim Craton by underplating of mantle plume-derived magmas: evidence from Neoproterozoic granitoids in the Kuluketage area, NW China. Precambrian Res. 187, 1–14.

Ludwig KR, 2003. User's manual for Isoplot 3.00: a geochronological toolkit for Microsoft Excel. Kenneth R. Ludwig.

Lu, S.N., 1992. The Proterozoic tectonic evolution of Kuruketage, Xinjiang. J. Tianjin Geol. Mineral Resour. 26–27, 279–292 (in Chinese with English abstract).

Lu, S.N., Li, H.K., Zhang, C.L., Niu, G.H., 2008. Geological and geochronological evidence for the Precambrian evolution of the Tarim craton and surrounding continental fragments. Precambrian Res. 160, 94–107.

Ma, S.P., Wang, Y.Z., Fang, X.L., 1989. The Sinian at the north slope western Kunlun Mountains. Xinjiang Geol. 7, 68–79 (in Chinese with English abstract).

Ma, S.P., Wang, Y.Z., Fang, X.L., 1991. Basic characteristics of Proterozoic Eonothem as a cover on north slope of Western Kunlun Mountains. Xinjiang Geol. 9, 59–71 (in Chinese with English abstract).

Nowell, G.M., Kempton, P.D., Noble, S.R., Fitton, J.G., Saunders, A.D., Mahoney, J.J., 1998. High precision Hf isotope measurements of MORB and OIB by thermal ionisation mass spectrometry: insights into the depleted mantle. Chem. Geol. 149, 211–233.

Park, S., Lee, H., Han, H., Lee, G., Kim, D., Yoo, D., 2000. Evolution of late quaternary mud deposits and recent sediment budget in the southeastern Yellow Sea. Mar. Geol. 170, 271–288.

Sun, W.H., Zhou, M.F., Gao, J.F., Yang, Y.H., Zhao, X.F., Zhao, J.H., 2009. Detrital zircon U–Pb geochronological and Lu–Hf isotopic constraints on the Precambrian magmatic and crustal evolution of the western yangtze block, SW China. Precambrian Res. 172, 99–126.

Scherer, E., Munker, C., Mezger, K., 2001. Calibration of the lutetium–hafnium clock. Science 293, 683–687.

Spencer, C.J., Cawood, P.A., Hawkesworth, C.J., Prave, A.R., Roberts, N.M.W., Horstwood, M.S.A., Whitehouse, M.J., EIMF, 2015. Generation and preservation of continental crust in the Grenville Orogeny. Geosci. Front. 16, 12–27.

Shu, L.S., Deng, X.L., Ma, D.S., Xiao, W.J., et al., 2011. Precambrian tectonic evolution of the Tarim Block, NW China: new geochronological insights from the Quruqtagh domain. J. Asian Earth Sci. 42, 774–790.

Tong, Q.L., Wei, W., Xu, B., 2013. Neoproterozoic sedimentary facies and glacial periods in the southwest Tarim block. Sci. China Ser. D 56, 901–912.

Turner, S.A., 2010. Sedimentary record of Late Neoproterozoic rifting in the NW Tarim Basin, China. Precambrian Res. 181, 85–96.
Wang, Y.Z., 2000. Paleogeography of the Meso-Neoproterozoic in Xinjiang. Xinjiang Geol. 18, 297–300 (in Chinese with English abstract).
Wang, C., Wang, Y.H., Liu, L., He, S.P., Li, R.S., Li, M., Yang, W.Q., Cao, Y.-T., Meert, J.G., Shi, C., 2014. The Paleoproterozoic magmatic–metamorphic events and cover sediments of the Tiekelik Belt and their tectonic implications for the southern margin of the Tarim Craton, northwestern China. Precambrian Res. 254, 210–225.
Wang, C., Liu, L., Wang, Y.H., He, S.P., Li, R.S., Li, M., Yang, W.Q., Cao, Y.T., Collins, A.S., Shi, C., Wu, Z.N., 2015. Recognition and tectonic implications of an extensive Neoproterozoic volcano-sedimentary rift basin along the southwestern margin of the Tarim Craton, northwestern China. Precambrian Res. 257, 65–82.
Wang, A.G., Zhang, C.L., Zhao, Y., Guo, K.Y., Dong, Y.G., 2004. Depositional types of the lower part of the Nanhua system at the northern margin of the SW Tarim and its tectonic significance. J. Stratigr. 28, 248–256 (in Chinese with English abstract).
Wu, F.Y., Yang, Y.H., Xie, L.W., Yang, J.H., Xu, P., 2006. Hf isotopic compositions of the standard zircons and baddeleyites used in U–Pb geochronology. Chem. Geol. 234, 105–126.
Wu, G.H., Chen, Z.Y., Qu, Y.L., Zhang, C.Z., 2012. SHRIMP zircon age of the high aeromagnetic anomaly zone in central Tarim Basin and its geological implications. Nat. Sci. 4 (1), 1–4.
Xinjiang, B.G.M.R., 1993. Regional Geology of the Xinjiang Uygur Autonomous Region. Geological Publishing House, Beijing, pp. 17–45.
Xu, B., Jiang, P., Zheng, H.F., Zou, H.B., Zhang, L.F., Liu, D.Y., 2005. U–Pb zircon geochronology of Neoproterozoic volcanic rocks in the Tarim Block of northwest China: implications for the breakup of Rodinia supercontinent and Neoproterozoic glaciations. Precambrian Res. 136, 107–123.
Xu, B., Xiao, S.H., Zou, H.B., Chen, Y., Li, Z.X., Song, B., Liu, D.Y., Zhou, C.M., Yuan, X.L., 2009. SHRIMP zircon U–Pb age constraints on Neoproterozoic Quruqtagh diamictites in NW China. Precambrian Res. 168, 247–258.
Xu, B., Zou, H.B., Chen, Y., He, J.Y., Wang, Y., 2013a. The Sugetbrak basalts from northwestern Tarim Block of northwest China: Geochronology, geochemistry and implications for Rodinia breakup and ice age in the Late Neoproterozoic. Precambrian Res. 236, 214–226.
Xu, Z.Q., He, B.Z., Zhang, C.L., Zhang, J.X., Wang, Z.M., Cai, Z.H., 2013b. Tectonic frame-work and crustal evolution of the Precambrian basement of the Tarim Block in NW China: new geochronological evidence from deep drilling samples. Precambrian Res. 235, 150–162.
Ye, H.M., Li, X.H., Li, Z.X., Zhang, C.L., 2008. Age and origin of the high Ba–Sr granitoids from northern Qinghai-Tibet plateau: implications for the early Paleozoic tectonic evolution of the Western Kunlun orogenic belt. Gondwana Res. 13, 126–138.
Ye, X.T., Zhang, C.L., Santosh, M., Zhang, J., Fan, X.K., Zhang, J.J., 2016. Growth and evolution of Precambrian continental crust in the southwestern Tarim terrane: new evidence from the ca.1.4 Ga A-type granites and Paleoproterozoic intrusive complexg. Precambrian Res. 275, 18–34.
Yong, W., Zhang, L., Hall, C., Mukasa, S., Essene, E., 2013. The $^{40}Ar/^{39}Ar$ and Rb–Sr chronology of the Precambrian Aksu blueschists in western China. J. Asian Earth Sci. 63, 197–205.
Yuan, C., Sun, M., Yang, J.S., Zhou, H., Zhou, M.F., 2004. Nb-depleted, continental rift-related Akaz metavolcanic rocks (West Kunlun): implication for the rifting of the Tarim Craton from Gondwana. Geol. Soc. 226, 131–143 (London, Special Publications).
Zhang, C.L., Zhao, Y., Guo, K.Y., Dong, Y.G., Wang, A.G., 2003a. Grenville orogeny in north of the Qinghai-Tibet plateau: first evidence from isotope dating. Chin. J. Geol. 38, 535–538 (in Chinese with English abstract).
Zhang, C.L., Dong, Y.G., Zhao, Y., 2003b. Geochemistry of Meso-Proterozoic volcanics in Western Kunlun: evidence for the plate tectonic evolution. Acta Geol. Sin. 77, 237–245.
Zhang, C.L., Li, Z.X., Li, X.H., Wang, A.G., Guo, K.Y., 2006. Neoproterozoic bimodal intrusive complex in southwestern Tarim block of NW China: age, geochemistry and Nd isotope and implications for the rifting of Rodinia. Int. Geol. Rev. 48, 112–128.
Zhang, C.L., Li, X.H., Li, Z.X., Lu, S.N., Ye, H.M., Li, H.M., 2007a. Neoproterozoic ultramafic–mafic–carbonatite complex and granitoids in Quruqtagh of northeastern Tarim Block, western China: geochronology, geochemistry and tectonic implications. Precambrian Res. 152, 149–169.
Zhang, C.L., Lu, S.N., Yu, H.F., Ye, H.M., 2007b. Tectonic evolution of Western Orogenic belt: evidences from zircon SHRIMP and LA-ICP-MS U–Pb ages. Sci. China Ser. D 50, 1–12.
Zhang, C.L., Li, Z.X., Li, X.H., Ye, H.M., 2007c. Early Paleoproterozoic high-K intrusive complex in southwestern Tarim Block, NW China: age, geochemistry and implications for the Paleoproterozoic tectonic evolution of Tarim. Gondwana Res. 12, 101–112.
Zhang, C.L., Li, Z.X., Li, X.H., Ye, H.M., 2009. Neoproterozoic mafic dyke swarm in north margin of the Tarim, NW China: age, geochemistry, petrogenesis and tectonic implications. J. Asian Earth Sci. 35, 167–179.
Zhang, C.L., Yang, D.S., Wang, H.Y., 2010. Neoproterozoic mafic dyke swarm and basalt in southern margin of the Tarim Block: age, geochemistry and their geodynamic implications. Acta Geol. Sin. 84, 549–562.
Zhang, C.L., Yang, D.S., Wang, H.Y., Takahashi, Y., Ye, H.M., 2011. Neoproterozoic ultramfic–mafic layered intrusion in Quruqtagh of northeastern Tarim Block, NW China: Two phases of mafic igneous activity of different mantle sources. Gondwana Res. 19, 177–190.
Zhang, C.L., Li, H.K., Santosh, M., Li, Z.X., Zou, H.B., Wang, H.Y., Ye, H.M., 2012a. Precambrian evolution and cratonization of the Tarim Block, NW China: Petrology, geochemistry, Nd-isotopes and U–Pb zircon geochronology from Archaean gabbro-TTG-potassic granite suite and Paleoproterozoic metamorphic belt. J. Asian Earth Sci. 47, 5–20.
Zhang, C.L., Zou, H.B., Li, H.K., Wang, H.Y., 2012b. Multiple phases of Neoproterozoic ultramafic–mafic complex in Kuruqtagh, northern margin of Tarim: interaction between plate subduction and mantle plume? Precambrian Res. 222–223, 488–502.
Zhang, C.L., Zou, H.B., Li, H.K., 2013. Tectonic framework and evolution of the Tarim Block, NW China. Gondwana Res. 23, 1306–1315.
Zhang, C.L., Zou, H.B., Santosh, M., Ye, X.T., Li, H.K., 2014a. Is the Precambrian basement of the Tarim Craton in NW China composed of discrete terranes? Precambrian Res. 254, 226–244.
Zhang, J., Zhang, C.L., Li, H.K., Ye, X.T., Geng, J.Z., Zhou, H.Y., 2014b. Revisit to the time and tectonic environment of the Aksu blueschist terrane in northern Tarim, NW China: New evidences from zircon U–Pb age and Hf isotope. Acta Petrol. Sin. 30, 3357–3365 (in Chinese with English abstract).
Zhao, G.C., Cawood, P.A., Wilde, S.A., Sun, M., 2002. Review of global 2.1–1. 8 Ga orogens: implications for a pre-Rodinia supercontinent. Earth Sci. Rev. 59, 125–162.
Zhao, G.C., Li, S.Z., Sun, M., Wilde, S.A., 2011. Assembly, accretion, and break-up of the Palaeo-Mesoproterozoic Columbia supercontinent: records in the North China Craton revisited. Int. Geol. Rev. 53, 1331–1356.
Zhao, G.C., Cawood, P.A., 2012. Precambrian geology of the North China, South China and Tarim Cratons. Precambrian Res. 222–223, 13–54.
Zhan, S., Chen, Y., Xu, B., Wang, B., Faure, M., 2007. Late Neoproterozoic paleomagnetic results from the Sugetbrak Formation of the Aksu area, Tarim basin (NW China) and their implications to paleogeographic reconstructions and the snowball Earth hypothesis. Precambrian Res. 154, 143–158.
Zheng, Y.F., Zhang, S.B., Zhao, Z.F., Wu, Y.B., Li, X.H., Li, Z.X., Wu, F.Y., 2007. Contrasting zircon Hf and O isotopes in the two episodes of Neoproterozoic granitoids in South China: implications for growth and reworking of continental crust. Lithos 96, 127–150.
Zheng, Y.F., Xiao, W.J., Zhao, G.C., 2013. Introduction to tectonics of China. Gondwana Res. 23, 1189–1206.
Zhu, W.B., Zhang, Z.Z., Shu, L.S., Lu, H.F., Sun, J.B., Yang, W., 2008. SHRIMP U–Pb zircon geochronology of Neoproterozoic Korla mafic dykes in the northern Tarim Block, NW China: implications for the long-lasting breakup process of Rodinia. J. Geol. Soc. 165, 887–890.